1 **Improvement of RAMS precipitation forecast at the short-range through lightning data**

2 **assimilation**

3 Stefano Federico[1], Marco Petracca[1], Giulia Panegrossi[1], Stefano Dietrich[1]

4 [1] *ISAC-CNR, UOS of Rome, via del Fosso del Cavaliere 100, 00133-Rome, Italy*

5 Phone: +390649934209

6 Fax: +390645488291

7 s.federico@isac.cnr.it

8 marco.petracca@artov.isac.cnr.it

9 g.panegrossi@isac.cnr.it

10 s.dietrich@isac.cnr.it

11 www.isac.cnr.it

Abstract

14 This study shows the application of a total lightning data assimilation technique to the RAMS

15 (Regional Atmospheric Modeling System) forecast. The method, which can be used at high

16 horizontal resolution, helps to initiate convection whenever flashes are observed by adding water

17 vapour to the model grid column. The water vapour is added as a function of the flash rate, local

18 temperature and graupel mixing ratio. The methodology is set up to improve the short-term (3h)

19 precipitation forecast and can be used in real-time forecasting applications. However, results are

20 also presented for the daily precipitation for comparison with other studies.

21 The methodology is applied to twenty cases that occurred in fall 2012, which were characterized by

22 widespread convection and lightning activity. For these cases a detailed dataset of hourly

23 precipitation containing thousands of rain gauges over Italy, which is the target area of this study, is

24 available through the HyMeX (HYdrological cycle in the Mediterranean Experiment) initiative.

25 This dataset gives the unique opportunity to verify the precipitation forecast at the short range (3h)

26 and over a wide area (Italy).

27 Results for the 27 October case study show how the methodology works and its positive impact on

28 the 3h precipitation forecast. In particular, the model represents better convection over the sea using

29 the lightning data assimilation and, when convection is advected over the land, the precipitation

30 forecast improves over the land. It is also shown that the precise location of convection by lightning

31 data assimilation, improves the precipitation forecast at fine scales (meso-β).

The application of the methodology to twenty cases gives a statistically robust evaluation of the impact of the total lightning data assimilation on the model performance. Results show an improvement of all statistical scores, with the exception of the Bias. The Probability of Detection (POD) increases by 3-5% for the 3h forecast and by more than 5% for daily precipitation, depending on the precipitation threshold considered.

Score differences between simulations with or without data assimilation are significant at 95% level for most scores and thresholds considered, showing the positive and statistically robust impact of the lightning data assimilation on the precipitation forecast.

Key words: total lightning data assimilation, forecast verification, convective storms, cloud resolving model.

1. Introduction

The inclusion of the effects of deep convection in the initial conditions of Numerical Weather Prediction (NWP) models is one of the most important problem to reduce the spin-up time and to improve initial conditions (Stensrud and Fritsch, 1994; Alexander et al., 1999). In recent years, several studies have shown the positive impact that lightning assimilation has on the weather forecast, and especially on the precipitation forecast (Alexander et al. 1999; Chang et al., 2001; Papadopulos et al., 2005; Mansell et al., 2007; Fierro et al., 2012; Giannaros et al., 2016).

Lightning data are a proxy for identifying the occurrence of deep convection, which relates to convective precipitation (Goodman et al., 1988). In addition to their ability to locate precisely the deep convection and heavy precipitation, lightning data have several advantages: availability in real time with few gaps (reliability), compactness (a low band is required to transfer the data), long-range detection of storms over the oceans and beyond the radars (Mansell et al., 2007).

Because of these properties, several techniques have been developed, in recent years, to assimilate lightning data in NWP. In the first studies (Alexander et al. 1999; Chang et al., 2001), lightning were used in conjunction with rainfall estimates from microwave data of polar orbiting satellites to derive a relation between the cloud to ground flashes and rainfall. Then the rainfall estimated from lightning was converted to latent heat nudging, that was assimilated in NWP (Jones and Macperson, 1997). These experiments showed a positive impact of the lightning data assimilation on the 12-24 h weather forecast.

Papadopulos et al. (2005) nudged relative humidity profiles associated with deep convection and the adjustment was proportional to the flash rate observed by the ZEUS network (Lagouvardos et

al., 2009). A modification of the Kain-Fritsch (Kain and Fritsch, 1993) convective parameterization in COAMPS (Coupled Ocean-Atmosphere Mesoscale Prediction System; Hodur, 1997) was introduced by Mansell et al. (2007). They enabled lightning to control the cumulus parameterization scheme activation. Recently, Giannaros et al. (2016) implemented a similar approach in the WRF model, showing the positive and statistically robust impact of the lightning data assimilation on the 24h rainfall forecast for eight convective events over Greece. Fierro et al. (2012) and Qie et al. (2014) introduced two lightning data assimilation schemes for the WRF model intervening on the mixing ratios of the hydrometeors (water vapour in the case of Fierro et al. (2012), and ice crystals, graupel and snow in Qie et al. (2014)). Both studies, which are performed at cloud resolving scales, show that lightning assimilation improves the precipitation forecast.

Most of the studies cited above are based on a case study approach. However, Giannaros et al. (2016) applied the methodology to eight convective cases that occurred in Greece from 2010 to 2013. Considering a larger number of cases allowed them to statistically test the improvement of the precipitation forecast through lightning data assimilation. Moreover, their methodology is designed to be realistic and usable in the operational forecast.

In a recent study, Federico et al. (2014) introduced a scheme to simulate lightning in RAMS (Regional Atmospheric Modeling System). Because the lightning distribution is well correlated to areas of deep convection, they concluded that lightning simulation can be a useful tool to evaluate the reliability of the NWP forecast in real time. In their study, however, lightning observations were used as a diagnostic tool.

In this paper, a total lightning data assimilation algorithm is used in the RAMS model. The assimilation scheme is similar to that of Fierro et al. (2012), with few modifications to account for different spatial and temporal resolutions of the two studies and for the different model suites. In addition, the methodology presented in this paper is designed to be used in real time NWP. This paper considers the short-term forecast (3h), even if the results for daily precipitation, accumulated from the 3h precipitation forecast, are also shown for completeness and for comparison with other studies.

To evaluate statistically the impact of the lightning data assimilation on the precipitation forecast, we consider twenty convective cases that occurred in fall 2012 over Italy, which is the target area of this study. Most of these events occurred during the HyMeX SOP1 (Hydrological cycle in the Mediterranean Experiment − First Special Observing Period), which was held from 5 September 2012 to 6 November 2012.

97   HyMeX (Drobinski et al., 2014; Ducroq et al., 2014) is an international experimental program that
98   aims to advance scientific knowledge of water cycle variability in the Mediterranean basin. This
99   goal is pursued through monitoring, analysis and modeling of the regional hydrological cycle in a
100 seamless approach. In HyMeX special emphasis is given to the topics of the occurrence of heavy
101 precipitation and floods, and their societal impacts, which were the subjects of the SOP1. One of the
102 products of the HyMeX-SOP1 is a database of hourly precipitation available for 2944 raingauges
103 over Italy belonging to the Italian DPC (Department of Civil Protection; Davolio et al., 2015). This
104 database extends behind the period of the HyMeX-SOP1 and contains all the events considered in
105 this paper.

106 The paper is organized as follows: Section 2 shows the RAMS configuration, the methodology used
107 to assimilate total lightning data, and the strategy used in the simulations. Section 3 gives the
108 results: first a case study of deep convection occurred over Italy during HyMeX-SOP1 is considered
109 to show how the lightning data assimilation works (Section 3.1); then the scores for the twenty
110 cases are shown in Section 3.2, which also shows the statistical robustness of the difference
111 between the precipitation forecasts of the simulations with or without total lightning data
112 assimilation. The discussion and conclusions are given in Section 4.

113

2. Methodology

2.1 The RAMS model configuration

116 The RAMS model is used in this study. This section is a brief description of the model setup, while
117 details on the model are given in Cotton et al. (2003).

118 We use two one-way nested domains at 10 km (R10) and 4 km (R4) horizontal resolutions,
119 respectively (Figure 1). The model is configured with thirty-six terrain following vertical levels for
120 both domains. The model top is at 22400 m (about 40 hPa). The distance of the levels is gradually
121 increased from 50 m to 1200 m. Below 1000 m the spacing between levels is less than 200 m,
122 above 5000 m the distance between levels is 1200 m.

123 The Land Ecosystem-Atmosphere Feedback model (LEAF) is used to calculate the exchange
124 between soil, vegetation, and atmosphere (Walko et al., 2000). LEAF uses a patch representation of
125 surface features (vegetation, soil, lakes and oceans, and snow cover) and includes several terms
126 describing their interactions as well as their exchanges with the atmosphere.

127 Explicitly resolved precipitation is computed by the WRF (Weather Research and Forecasting
128 System) – single-moment six-class microphysics scheme (WSM6; Hong et al., 2006). This scheme

129 was recently implemented in RAMS (Federico, 2016) and showed the best performance among the

130 microphysics schemes available in the model for a forecast period spanning 50 days of the HyMeX-

131 SOP1 at 4 km horizontal resolution. The WSM6 scheme accounts for the following water variables:

132 vapour, cloud water, cloud ice, rain, snow and graupel. The best configuration of Federico (2016) is

133 used in this paper and is hereafter referred to as control (CNTRL).

134 Sub-grid-scale effect of clouds is parameterized following Molinari and Corsetti (1985). They

135 proposed a form of the Kuo scheme (Kuo, 1974) accounting for updrafts and downdrafts. The

136 convective scheme is applied to the 10 km grid only.

137 The unresolved transport is parametrized by the K-theory following Smagorinsky (1963), which

138 relates the mixing coefficients to the fluid strain rate and includes corrections for the influence of

139 the Brunt-Vaisala frequency and the Richardson number (Pielke, 2002).

140 The Chen and Cotton (Chen and Cotton, 1983) scheme is used to compute short and long-wave

141 radiation. The scheme accounts for condensate in the atmosphere, but not for the specific

142 hydrometeor type.

143 The initial and dynamic boundary conditions are introduced in section 2.3.

144 Before concluding this section, it is important to note that 4 km horizontal resolution of the finer

145 grid corresponds to the grey area for convection and it is slightly below actual standards (2-3 km).

146 This resolution was motivated by operational purposes: the methodology of this paper is

147 implemented in a real-time weather forecasting system at ISAC-CNR and we study the performance

148 of this specific system. Preliminary results of the impact of the horizontal resolution on the

149 lightning assimilation are discussed in Section 4.

150 *2.2 Lightning data and assimilation procedure*

151 Lightning data used in this paper are those observed by LINET (LIghtning detection NETwork;

152 Betz et al., 2009), which is a European lightning location network for high-precision detection of

153 total lightning, cloud to ground (CG) and intra cloud (IC) lightning, with utilization of VLF/LF

154 techniques (in range between 1 and 200 KHz).

155 The network has more than 550 sensors in several countries worldwide, with very good coverage

156 over central Europe and central and western Mediterranean (from 10° W to 35° E in longitude and

157 from 30° N to 65° N in latitude). The lightning three-dimensional location is detected using the time

158 of arrival (TOA) difference triangulation technique (Betz et al., 2009). The lightning strokes are

159 detected with high precision (150 m for an average distance between sensors of 200 km) in both

160 horizontal and vertical directions. The LINET "strokes" are grouped into "flashes" before

161   assimilation in the model. In particular, all events recorded by LINET that occur within 1 s and in

162   an area with a radius of 10 km are binned into a single flash (Federico et al., 2014).

163   Observed flashes are mapped onto the RAMS grid for assimilation in space and time. In particular,

164   the assimilation procedure computes the number of flashes occurring in each RAMS grid cell in the

165   past five minutes (X). Then the water vapour mixing ratio is computed as:

166 $$q_v = Aq_s + B*q_s*tanh(CX)*(1-tanh(DQ_g^{\alpha})) \qquad (1)$$

167   Where A=0.86, B=0.15, C=0.30 D=0.25, α=2.2, q_s is the saturation mixing ratio at the model

168   atmospheric temperature, and Q_g is the graupel mixing ratio (g kg^{-1}). The water vapour mixing ratio

169   derived from Eqn. (1) is similar to Fierro et al. (2012). There are two changes: first the C coefficient

170   is larger in this study (in Fierro et al. (2012), C=0.01), which partially accounts for the different

171   horizontal resolutions of the remapped observed flashes (9 km in Fierro et al., (2012); 4 km in our

172   case, corresponding to the RAMS inner grid horizontal resolution) and for the different grouping

173   time interval (10 minutes in Fierro et al. (2012), and 5 minutes here). Second, the coefficient A (B)

174   is larger (smaller) in this study compared to Fierro et al. (2012; A=0.81 and B=0.20) because we

175   find a better performance with this setup. The set-up of Eqn. (1) was found by trials and errors

176   analysis for two case studies (15 and 27 October 2012) and considering two opposite needs: to

177   increase the precipitation hits and to reduce (or not increase considerably) the false alarms. It is

178   noted that Fierro et al. (2012) found little sensitivity of the results by varying A by 5%.

179   The water vapour derived from Eqn. (1) is substituted to the simulated value at a grid point where

180   electric activity is observed and RH is below 86%. By this choice we only add water vapour to the

181   simulated field, leaving it unchanged if the simulated water vapour is larger than that of Eqn. (1).

182   Moreover, the water vapour is substituted only in the charging zone (from 0 to -25 °C), which is the

183   mixed-phase graupel-rich zone associated with electrification and lightning activity (MacGorman

184   and Rust, 1998). The increase of q_v, Eqn. (1), is inversely proportional to the simulated graupel

185   mixing ratio. When Q_g is 3 g/kg the second term of the right hand side of Eqn. (1) is ineffective (see

186   Figure 7 of Fierro et al. (2012) for the dependency of Eqn. (1) on the graupel mixing ratio). For a

187   given value of Q_g between 0 and 3 g/kg, the water vapour of Eqn. (1) increases as a function of the

188   gridded flash rate X.

189   It is noted that we change the water vapour in the charging zone between 0°C and -25°C, without a

190   relaxing zone. The water vapour, however, is redistributed by the model advection, diffusion and

191   diabatic processes, and is considerably changed outside the charging zone (see the discussion of this

192   paper; Federico et al. 2016).

193

2.3 Simulation strategy and verification

Twenty case studies that occurred in fall 2012 were selected. The events are reported in Table 1 and were all characterized by widespread convection, lightning activity, and moderate-heavy precipitation over Italy. The events of Table 1 comprise eight of the nine IOP (Intense Observing Period) declared in Italy (see Table 5 of Ferretti et al. (2014) for the complete list of the IOP) during HyMeX-SOP1 and few other cases of November 2012.

A 36 h forecast at 10 km horizontal resolution is performed for each case (R10). The initial and boundary conditions (BC) for this run are given by the 12 UTC assimilation/forecast cycle of the ECMWF (European Centre for Medium Weather range Forecast). Initial and BC are available at 0.25° horizontal resolution. The R10 forecast starts at 12 UTC of the day before the day of interest (actual day, Table 1) and the first 12 hours, which also account for the spin-up time, are discarded from the evaluation. The R10 forecast is made to give the initial and BC to the 4 km horizontal resolution forecast (R4), avoiding the abrupt change of resolution from the ECMWF initial conditions and BC (0.25°) to the R4 horizontal resolution.

Starting from R10 as initial and BC, three kind of simulations, all using the R4 configuration, are performed for each event: a) CNTRL: this simulation is performed by nesting R4 in R10 using a one-way nest and without doing lightning data assimilation. Each CNTRL simulation starts at 18 UTC of the day before the actual day and the first six hours, which account for the spin-up time, are discarded from the evaluation; b) F3HA6: these simulations consist of eight runs of 9 h duration. During the first 6 h, lightning data are assimilated following the procedure described in the previous section. Then, a short term 3 h forecast is made. Eight F3HA6 simulations are needed to span the forecast of a whole day (Figure 2). The first simulation starts at 18 UTC of the day before the actual day, using as initial and boundary conditions the R10 forecast, and gives the forecast for the hours 00-03 UTC of the actual day. The second F3HA6 simulation starts at 21 UTC of the day before the actual day using as initial conditions the previous R4 forecast, belonging to F3HA6 set of simulations, and as BC the R10 forecast. Lightning are assimilated from 21 UTC of the day before to 03 UTC of the actual day, while the forecast is valid for 03-06 UTC of the actual day. The F3HA6 forecasts from three to eight proceed as the second but shifted every time three hours ahead. Please note the switch of the initial conditions between the first and second F3HA6 simulations from R10 to R4. This is done to maximise the impact of lightning data assimilation on the F3HA6 run, since the initial conditions provided by R4 are produced by a simulation using lightning data, while in R10 lightning data are not used; c) ASSIM: this simulation is performed by nesting R4 in

226   R10 using a one-way nest and doing lightning data assimilation for the whole run. Each ASSIM

227   simulation starts at 18 UTC of the day before the actual day and the first six hours of forecast are

228   considered as spin-up time and are discarded from the evaluation. The ASSIM simulation

229   continuously assimilates lightning data and, because it represents better convection during the

230   events compared to CNTRL and F3HA6, has the best performance (Section 3.2). The ASSIM

231   configuration can be useful when analysing the events but cannot be used for the forecast because it

232   needs real-time lightning data as the integration time advances.

233   It is noted that the configuration F3HA6 was chosen because it can be applied in the operational

234   context. The simulation R10 takes less than one hour to complete the 36 h forecast on a 64 core

235   state of the art cluster. Each simulation F3HA6 takes 20-25 minutes using a 64 cores state of the art

236   cluster, which makes the forecast available for operational purposes. Continuous advancing of

237   computing power will give the possibility to apply the methodology at finer horizontal resolutions

238   for extended areas, as that considered in this paper, as well as to reach the kilometric scale for

239   limited areas.

240   Even if the main focus of this paper is on the short-term (3 h) forecast, the daily precipitation

241   accumulated from the 3h forecasts is also considered for comparison with other studies available in

242   the literature. For F3HA6 the daily precipitation is given by adding the eight 3 h forecasts available

243   for the actual day (Figure 2).

244   One of the products of the HyMeX initiative is a database of hourly precipitation from the network

245   of the DPC of Italy, which consists of 2944 rain gauges all over Italy. The dataset is available at

246   http://mistrals.sedoo.fr/?editDatsId=1282&datsId=1282&project_name=MISTR&q=DPC and it is

247   used to derive 3 h and daily rainfall, which are then used to verify the model.

248   For the verification of the Quantitative Precipitation Forecast (QPF), the model output at the closest

249   grid point of a raingauge is considered. When two or more raingauge fall in the same model grid-

250   cell, the average precipitation recorded by these raingauges is considered.

251   Statistical verification is performed by 2x2 contingency tables for different precipitation thresholds.

252   For the 3 h rainfall comparison the thresholds are: 0.2, 1.0, 3.0, 5.0, 7.5, 10.0, 15.0, 20 mm/3h. For

253   daily precipitation the thresholds are: 1, 5, 10, 20, 40, 60 mm/day, with 60 mm/day (7.5 mm/3h)

254   considered as the threshold for severe precipitation events in the Mediterranean Basin (Jansà et al.,

255   2014). From the hits (*a*), false alarms (*b*), misses (*c*), and correct no forecasts (*d*) of the contingency

256   tables, the probability of detection (POD; range [0, 1], where 1 is the perfect score, i.e. when no

257   misses and false alarms occur), the False Alarm Ratio (FAR; range [0, 1], where 0 is the perfect

258 score), the Bias (range [0, + ∞), where 1 is the perfect score) and the equitable threat score (ETS;

259 range [-1/3,1], where 1 is the perfect score and 0 is a useless forecast) are computed (Wilks, 2006):

260
$$POD = \frac{a}{a+c}$$
$$FAR = \frac{b}{a+b}$$
$$Bias = \frac{a+b}{a+c}$$
$$ETS = \frac{a-a_r}{a+b+c-a_r}; \quad and \quad a_r = \frac{(a+b)(a+c)}{a+b+c+d}$$

(1)

261 where a_r is the probability to have a correct forecast by chance (Wilks, 2006).

262 The POD gives the fraction of the observed rain events that were correctly forecast. The FAR gives

263 the fraction of rain forecast events that didn't occur. The Bias tells us the fraction of rain forecast

264 events with respect to the rain observed events. The ETS measures the fraction of observed and/or

265 forecast rain events that were correctly predicted, adjusted for hits associated to a random forecast,

266 where the forecast occurrence/non-occurrence is independent of observation/non observation.

267 In order to have a measure of the difference between the CNTRL and F3HA6 forecast, a hypothesis

268 test to verify that the score difference between the two competing models is significant at a

269 predefined significance level (90%, α=0.1; or 95%, α=0.05) is made. The test was originally

270 proposed by Hamill (1999), is based on resampling, and is discussed in Appendix A.

271

272 **3. Results**

273

274 *3.1 The 27 October 2012 case study*

275 The event studied in this section is taken from the HyMeX SOP1 campaign, which was focused on

276 heavy precipitation and its societal impact (Ducroq et al., 2014; Ferretti et al., 2014). Nine of the

277 twenty IOPs (Intense Observing Period) considered in SOP1 occurred in Italy.

278 During SOP1, several upper level troughs extended from the Northern and Central Europe toward

279 the Mediterranean Basin or entered in the Basin as deep trough. Few of them developed a cut-off

280 low at 500 hPa; the interaction between the upper level troughs and the orography of the Alps

281 generated a low pressure pattern at the surface in Northern Italy, and usually the whole system

282 moved along the Italian peninsula. The 27 October 2012 case study, also referred as IOP16a,

belongs to this class of events, and it eventually evolved in a cut-off at 500 hPa on 28-29 October (IOP16c). This event, characterized by widespread convection and intense lightning activity, caused huge precipitation all along the peninsula and also peak values of water level on the Venice Lagoon, where the sea level exceeded twice the warning level of 120 cm (Casaioli et al., 2013; Mariani et al., 2014).

Figure 3 shows the synoptic situation at 12 UTC on 27 October 2012. At 500 hPa, Figure 3a, a trough extends from NE Europe toward the Western Mediterranean. The interaction between the trough and the Alps generated a mesolow over northern Italy, as shown by the 990 hPa contour in Figure 3b, that caused a cyclonic circulation over most of the peninsula.

In these synoptic conditions, winds over the Tyrrhenian Sea are from W and SW and bring humid and unstable air over the mainland of Italy. The interaction between the unstable air and the orography of Italy reinforced convection, which, however, was already occurring over the sea as shown by the intense electric activity over the Tyrrhenian Sea (see below).

Figure 4a shows the lightning distribution observed by LINET on 27 October 2012. From Figure 4a, convection is apparent over the Tyrrhenian Sea and it is enhanced over land because of the interaction between the humid and unstable air masses from the sea and the orography of Italy.

The daily precipitation (Figure 4b), which is unavailable for a wide area of Central-Northern Italy, shows the widespread convection over the Apennines, with several stations reporting more than 90 mm/day. More than 200 mm are reported in two stations in Southern Italy (15.84E, 40.31N; 207 mm) and (15.98E, 40.16N; 220 mm), while the largest precipitation recorded in NE Italy is 141 mm (13.54E, 45.85N). Note also the abundant precipitation over Sardinia and over the North-East of Italy. It is important to note that the rainfall of Figure 4b is computed by summing the 1h precipitation registered by the rain gauges. If one of the 1h observations is unavailable, the raingauge does not appear in Figure 4b. So, when verifying the precipitation for shorter time scales, different rain gauges could appear compared to those of Figure 4b.

Figures 5a and 5b show the daily precipitation forecast of the CNTRL run and the daily accumulated precipitation of the F3HA6 run. Figures 5a and 5b shows a high precipitation amount over the Apennines (> 90 mm/day) all along the peninsula, in agreement with observations. However, the precipitation is overestimated by both CNTRL and F3HA6, especially above 30 mm/day. This is apparent by comparing the area of the 90 mm/day threshold in Figures 5a-5b with the comparatively few rain gauges reporting this precipitation amount. As it will be shown in the next section, this is a general behaviour of the RAMS model with the setup used in this paper. Other features shown by Figures 5a and 5b are: a very heavy precipitation spell in NE Italy, whose area is

overestimated by CNTRL and F3HA6; a high precipitation spell over the Liguria-Tuscany area, which is only partially revealed by observations due to the lack of data; a moderate precipitation over Sardinia, which is underestimated by the CNTRL forecast both for the precipitation area and amount.

Even if CNTRL and F3HA6 share several precipitation features in common, there are important differences between Figures 5a and 5b. Convection over the sea is underestimated by CNTRL. Even if we cannot prove it by the precipitation amount, the intense electrical activity over the Central Mediterranean Sea, and especially over the Tyrrhenian Sea, shows that the convective activity over the sea is underestimated by CNTRL.

Convection over the sea is simulated by F3HA6 thanks to the lightning data assimilation. When convection is advected over the land it increases the precipitation. This is clearly shown by the precipitation over Sardinia, which increases both in areal coverage and rainfall amount for F3HA6 compared to CNTRL.

Other differences between the precipitation field of CNTRL and F3HA6 can be discussed more easily by the difference of the precipitation fields. Figure 5c shows the precipitation difference between CNTRL and F3HA6 in this order, so that positive values show larger precipitation for CNTRL, while negative values show larger precipitation for F3HA6.

From Figure 5c it is apparent that the precipitation of F3HA6 increases over large areas of the domain, especially over the Tyrrhenian Sea. The rainfall over Sardinia increases up to 40 mm/day, showing the important impact of the lightning assimilation on the forecast. However, the largest differences are found along the Apennines with values up to 80 mm/day.

In general, the lightning assimilation increases the precipitation, nonetheless Figure 5c shows also areas where the precipitation of F3HA6 decreases compared to CNTRL, because of the different evolution of the storm in the two simulations. This is especially evident over the Adriatic coast of the Balkans where positive-negative patterns alternate every few tens of kilometres. We will discuss further this point later on in this section.

Up to now, we considered the impact of the lightning assimilation on the daily precipitation, i.e. when the rainfall of the eight F3HA6 forecasts in a day are added, however the main focus of this paper is on the short-term precipitation forecast. To consider this point, Figure 6a shows the observed precipitation accumulated between 06 and 09 UTC, and the corresponding precipitation for the CNTRL (Figure 6b) and F3HA6 (Figure 6c).

347   Figure 6a shows considerable precipitation spells (about 40 mm/3h) over NE Italy, in some spots

348   over the Apennines all along Italy, and, somewhat smaller, over Sardinia.

349   Comparing Figure 6b with Figure 6a it is apparent that the CNTRL forecast is able to catch several

350   features of the precipitation field, as the local spots of heavy rain over the Apennines or the rain

351   spell over NE Italy, the main error being the scarce precipitation simulated over Sardinia. This issue

352   is in part solved by the F3HA6 forecast (Figure 6c), which shows larger precipitation compared to

353   CNRTL over Sardinia.

354   To better focus on the improvement given by the lightning data assimilation on the short term QPF,

355   we consider the precipitation hits, i.e. the correct forecasts, of the contingency tables. Figure 7a

356   shows the difference between the hits of the F3HA6 and CNTRL (in this order) for the 1 mm/3h (8

357   mm/day) threshold. In Figure 7a, the +1 (red asterisk) shows a station where the CNTRL forecast

358   did not predict a precipitation equal or larger than the threshold, while the F3HA6 correctly

359   predicted a rainfall equal or larger than the threshold at the raingauge. The -1 value (blue asterisk)

360   shows the opposite behaviour. In Figure 7a there are fifty-two new correctly predicted events for

361   F3HA6. They are located in the Apennines and, mostly, over Sardinia, where CNTRL missed the

362   forecast (Figures 5a-5b). There are also two stations where the lightning assimilation worsens the

363   forecast, because of the different evolutions of the storms in CNTRL and F3HA6, nevertheless the

364   benefits of the lightning data assimilation on the short term QPF are apparent for the 1 mm/3h

365   threshold.

366   Figure 7b shows the difference between the hits of F3HA6 and CNTRL for the 10 mm/3h (80

367   mm/day) threshold, which is more interesting when considering moderate-high rainfall amounts.

368   For this threshold, the lightning data assimilation improves the forecast because twelve new events

369   are correctly predicted by F3HA6 along the Apennines and over Sardinia.

370   It is important to note the precision of the correction to the precipitation field given by the lightning

371   data assimilation. The positive-negative pattern of the difference between the precipitation fields of

372   CNTRL and F3HA6 (shown for the daily precipitation, Figure 5c, with amplitudes of tens of

373   kilometres in the Central Apennines) is found, with lower amplitude, also for the 3h forecast (not

374   shown). The F3HA6 forecast gave the correct prediction of several new stations for both 1 mm/3h

375   (fifty-two raingauges) and 10 mm/3h (twelve raingauges) thresholds, while losing only two stations

376   correctly predicted by CNTRL for the 1 mm/3h threshold. This shows that the precipitation is added

377   where necessary, but also that it is subtracted where it did not occur, i.e. only two correct forecasts

378   are lost by the lightning data assimilation. For example, between 03 and 06 UTC there are 110

379   stations where the precipitation is reduced by more than 1 mm/3h, 20 stations where it is reduced by

380   more than 5 mm/3h, and 7 stations for which the precipitation is reduced by more than 10 mm/3h.

381   It is worth noting that the stations correctly forecast by both CNTRL and F3HA6 for a given

382   precipitation threshold do not appear in Figures 7a and 7b. This occurs, for example, for the

383   raingauges in NE Italy.

384   This section showed how the data assimilation technique of this study works and how it is able to

385   add new correct forecasts (hits) to CNTRL for a case study. In the following section, scores based

386   on contingency tables are presented for a total of twenty case studies in order to quantify, in a

387   statistically robust way, the benefits of the total lightning data assimilation on the short-term QPF.

388

389   *3.2 Statistical scores*

390   In this section we discuss the statistical scores of the F3HA6 forecast in comparison to CNTRL.

391   The results of the ASSIM run are also presented as the benchmark for lightning data assimilation.

392   First we discuss the results for the daily precipitation accumulated starting from 3h rainfall

393   forecasts.

394   Figure 8a shows that the Bias increases with the threshold from 0.8-1.0 (1 mm/day threshold,

395   depending on the type of simulation) to 2.3-2.6 (60 mm/day threshold), showing a considerable

396   overestimation of the forecast area for the larger thresholds (> 40 mm/day). The lightning data

397   assimilation improves the Bias up to 10 mm/day (both F3HA6 and ASSIM), while performance is

398   worsened by data assimilation for larger thresholds. As expected, the ASSIM shows the largest

399   Bias, followed by F3HA6 and CNTRL. This is caused by the addition of water vapour by the data

400   assimilation, which is larger for ASSIM (assimilation performed continuously) compared to F3HA6

401   (assimilation is not performed in the forecast phase). The statistical test to assess the bias difference

402   between CNTRL and F3HA6 shows that the two scores are different at 95% significance level for

403   all thresholds, showing the significant impact of the lightning data assimilation on the precipitation

404   forecast.

405   The overestimation of the precipitation area for higher thresholds is well evident, as discussed in the

406   previous section, in Figures 5a-5b over the Apennines for the 90 mm/day threshold (the ASSIM

407   simulation, not shown, does not differ substantially from F3HA6). Comparing the result of the Bias

408   with the same result of Federico (2016), where the same configuration of the RAMS model of

409   CNTRL was used, we note a considerable increase of the Bias in this work. This difference is

410   caused by the fact that Federico (2016) considered 50 consecutive days of the HyMeX-SOP1, i.e.

411   with heavy, moderate and small precipitation, while this study considers only cases with deep and

widespread convection. The RAMS with WSM6 scheme shows the tendency to overestimate the Bias for increasing precipitation (Federico, 2016; see also Liu et al., 2011 for a general comparison of the WSM6 microphysical scheme and other microphysical schemes available in the Weather Research and Forecast (WRF) model), and this tendency is amplified for the heavy precipitation events considered in this work.

Figure 8b shows the ETS score. For CNTRL it decreases from 0.35 (1 mm/day) to 0.17 (60 mm/day). The ETS increases for F3HA6, especially for thresholds lower than 40 mm/day, showing the positive impact of the lightning assimilation on the precipitation forecast. The difference of the ETS for F3HA6 and CNTRL is statistically significant at 95% level for thresholds up to 20 mm/day, and not significant for larger precipitation. The ASSIM simulations show a further increase of the ETS compared to F3HA6 because of their ability to better represent convection during the simulation through lightning data assimilation.

The POD (Figure 8c) for CNTRL decreases from 0.70 (1 mm/day) to 0.52 (60 mm/day), i.e. half of the potentially dangerous events are correctly predicted. It is also noted the rather stable value of the POD (0.6) between the 10 and 40 mm/day thresholds. The POD increases for F3HA6. The lowest increment is attained for 60 mm/day (0.04, i.e. 4% more potentially dangerous events are correctly forecast compared to CNTRL), the largest for the 1 mm/day (6.5%). Differences between the POD of CNTRL and F3HA6 are significant at 95% level for all thresholds showing the robust improvement of the performance for this score using lightning data assimilation. Notably, the ASSIM run increases the POD of 8-10%, depending on the threshold.

The FAR for CNTRL (Figure 8d) increases from less than 0.2 (1 mm/day threshold; i.e. less than 20% of the forecasts are false alarms) to 0.8 (60 mm/day threshold; i.e. 80% of the forecasts are false alarms). The lightning assimilation improves the performance for the FAR but differences are statistically significant for 1 mm/day (90% level), 5 and 10 mm/day (95% level). The inspection of the contingency tables shows that the improvement of the FAR for those thresholds is attained by a larger number of hits but there is also an increase of the false alarms. In general, the lighting assimilation increases the precipitation, which is already overestimated for the larger thresholds by CNTRL. So, the POD and the hit rate are increased by lightning data assimilation, but also the false alarms, which were already reported in CNTRL, especially for the larger thresholds (> 30 mm/day). Anyway, we believe that the result is overall helpful for operational purposes.

Figure 9a shows the Bias for the 3h precipitation forecast. The Bias for CNTRL increases from about 1 (0.2 mm/3h threshold) to 2.5 (20 mm/3h threshold). The Bias differences between CNTRL and F3HA6 are significant at 95% level for all thresholds.

445 The ETS score (Figure 9b) for CNTRL shows a decrease from 0.33 (0.2 mm/3h threshold) to 0.13
446 (20 mm/3h threshold). The ETS is larger for F3HA6 compared to CNTRL and the differences of the
447 scores are significant at 95% level for all thresholds. It is also noted that, while the ETS is positive
448 for all thresholds, the ETS value is rather low for the 20 mm/3h threshold, limiting the usefulness of
449 the forecast.

450 Figure 9c shows the POD for the 3h forecast. The value for CNTRL decreases from 0.63 (0.2
451 mm/3h) to 0.43 (20 mm/3h). The POD increases for F3HA6, notably for thresholds up to 7.5
452 mm/3h (>5%), while the improvement is smaller (3%-4%) for larger thresholds.

453 Figure 9d shows the FAR for the 3h forecast. The FAR increases from 0.3 to 0.83 for the CNTRL
454 forecast. The FAR for F3HA6 decreases (1-3% depending on the threshold) and the improvement is
455 the result of the increase of the hits but it is also associated to an increase of the false alarms.

456

4. Discussion and conclusions

458 This study shows the application of a total lightning data assimilation technique, developed by
459 Fierro et al. (2012), to the RAMS model with WSM6 microphysics scheme (Federico, 2016). The
460 technique adds water vapour to grid columns where flashes are observed, and the water vapour
461 added at constant temperature depends on the flash rate and on the graupel mixing ratio. Water
462 vapour is added to the model when suitable, while the water vapour is unchanged when the model
463 predicts a value larger than that of the data assimilation algorithm. This paper shows a realistic
464 implementation of the assimilation/forecast procedure that can be adopted in operational weather
465 forecast.

466 The results of this paper show that the methodology is effective at improving the short-term (3h)
467 precipitation forecast. More in detail, the analysis of the 27 October shows that the total lightning
468 data assimilation is able to trigger convection over the sea and, when convection is advected over
469 the land, it improves the short-term precipitation forecast. This effect is apparent over Sardinia for
470 the case study. The humid marine air masses interact with the local orography causing or
471 reinforcing convection. Also, the lightning data assimilation improves the rainfall forecast adding
472 precipitation where it is observed and increasing the hits of the short-term forecast.

473 The advection of convection from the sea to the land was important in most case studies considered
474 in this paper, and we can conclude that it plays a fundamental role. There are cases, however, when
475 it is less important, as for the severe and localized storm that occurred in NE Italy on 12 September
476 2012 (Manzato et al., 2014). For this case, the storm developed and evolved over land, and the

477 difference between the precipitation field of the CNTRL and F3HA6 is confined inland, over NE
478 Italy, and it is larger than 40 mm (see the discussion of this paper for the map of the precipitation
479 difference between CNTL and F3HA6; Federico et al., 2016).

480 The analysis of the scores for the 3h precipitation forecast, computed for twenty cases characterized
481 by intense lightning activity and widespread convection, confirms the improvement of the
482 precipitation forecast using lightning data assimilation. The ETS and POD increase for all
483 thresholds considered for F3HA6 compared to CNTRL and the difference between the scores of the
484 competing forecasts is significant at 95% level for all thresholds. The FAR is also improved and the
485 difference between the scores of F3HA6 and CNTRL is statistically significant for all thresholds
486 with the exception of the 15 mm/3h. The FAR improvement of F3HA6 is caused by the increase of
487 the hits, but it is also associated to a larger number of false alarms.

488 The Bias is the only score that worsens with lightning data assimilation. The Bias of the RAMS
489 model with the WSM6 microphysics scheme is larger than one for most thresholds for the case
490 studies of this paper. Because the lightning data assimilation adds water vapour to the model, the
491 tendency to overestimate the precipitation area, especially for the larger thresholds, is worsened by
492 the lightning data assimilation.

493 In addition to the 3h forecast, the scores and precipitation field are analysed for the daily
494 precipitation for completeness and for comparison with other studies. Recently, Giannaros et al.
495 (2016) presented the WRF-LTNGDA, a lightning data assimilation technique implemented in
496 WRF. They presented the results for eight cases in Greece. Their assimilation strategy focuses on
497 the daily rainfall prediction (tomorrow daily precipitation). Their analysis (see their Figure 3, note
498 also that the maximum precipitation threshold is 20 mm/day in their study) shows that the POD
499 increases when lightning data assimilation is compared to CNTRL, and the increase of the POD is
500 up to 5%. Moreover, for some thresholds, the lightning assimilation lowers the POD because of the
501 different patterns followed by the storms in the simulations with or without lightning data
502 assimilation.

503 Our results show that the POD improves for all precipitation thresholds when lightning data
504 assimilation is used and the percentage of improvement is slightly better than that reported in
505 Giannaros et al. (2016) for the lower thresholds (below 10 mm/day). Even if we cannot give a
506 definitive answer to this issue, because of the many important differences between this study and
507 that of Giannaros et al. (2016), the lightning data assimilation technique has a role. In our case,
508 lightning data are assimilated also for the actual day (6h assimilation before the forecast start time
509 followed by 3h forecast, Figure 2), while in Giannaros et al. (2016) the assimilation is done only for

510   the day before the actual day (6h assimilation followed by 24 h forecast). So, our technique should

511   improve the correct location of convection during the actual day compared to their approach, as

512   shown by the improvement, i.e. the difference between the POD of the simulations with or without

513   lightning data assimilation.

514   However, other differences play a role: first the two studies refer to different regions and to

515   different events. In our case the extension of the region, the number of the events, and the number

516   of verifying stations are larger. Moreover, two different model suites are used (WRF and RAMS).

517   These differences are clearly seen in the score values. The POD of Giannaros et al. (2016), is larger

518   than that of this study, especially for thresholds lower than 20 mm/day. Another important

519   difference arises from the different convective nature of the storms considered in the two works.

520   The performance of the precipitation forecast is clearly dependent on the type of event, i.e.

521   widespread or localized convection (Giannaros et al., 2016) and, because the events considered in

522   the two studies are different, the comparison can be only qualitative. Nevertheless, both studies

523   show that the lightning data assimilation improves the precipitation forecast robustly, and can be

524   used in the operational context.

525   While the results of this study are encouraging, there are a number of issues that need further

526   investigation. The water vapour is added to the grid column where the lightning is observed.

527   However, the lightning is often the result of a process involving larger scales than the horizontal

528   grid spacing considered in this paper (4 km). A spatial extension of the influence of the lightning

529   perturbation on the water vapour field should be explored. For this approach the applications of the

530   methods involving the model error matrix are foreseeable and will be investigated in future studies.

531   The problem of the spatial extension of the water vapour perturbation caused by lightning to the

532   model was considered in Fierro et al. (2012) by remapping the flashes onto a coarser horizontal

533   resolution grid (9 km), while no similar approach is done in this study.

534   A problem arising with the RAMS model using the WSM6 microphysics scheme is the

535   overestimation of the precipitation area for large rainfall thresholds. This tendency was already

536   noted in Federico (2016), and it is amplified for the cases of widespread convection considered in

537   this study. The high number of false alarms decreases the ETS score for high precipitation, reducing

538   the applicability of the method for the largest thresholds (> 100 mm/day). The application of

539   different microphysical schemes could mitigate this issue.

540   Finally, horizontal resolutions higher than that of this paper are needed to better resolve the

541   orography and its interaction with air masses. To quantify this point preliminary, we increased the

542   horizontal resolution of the second domain from 4 km to 2.5 km for the 15 October and 27 October

543 case studies. Results for the two cases show that the impact of the resolution is notable because the

544 precipitation patterns, especially for larger thresholds (>50 mm/day), are less spread in the 2.5 km

545 horizontal resolution experiment compared to 4 km forecast (see the discussion of this paper for the

546 daily precipitation maps for the two cases, Federico et al., 2016). This impact could be beneficial

547 for the scores of the F3HA6 forecast because it has the tendency to overestimate the precipitation

548 area at high thresholds, as shown in this paper. However, these results are preliminary, and future

549 studies are needed to quantify the important impact of the horizontal resolution on the lightning data

550 assimilation forecast.

551

552 **Appendix A**

553 We use the resampling method introduced by Hamill (1999) for the comparison of the scores of

554 CNTRL and F3HA6 forecasts (see also Accadia et al. (2003) and Federico et al. (2003)).

555 The null hypothesis is that the difference of the scores of the two competing models, CNTRL and

556 F3HA6, is zero:

557 $$H_0: \; S_1 - S_2 = 0 \tag{A1}$$

558 Where S is the generic score (Bias, ETS, POD and FAR), 1 is the CNTRL forecast and 2 is the

559 F3HA6 forecast. The scores are computed from the sum of the contingency tables of the CNTRL

560 and F3HA6 forecasts to minimize the sensitivity of the test to small changes of the contingency

561 table elements.

562 In this paper the number of contingency tables available is 8 multiplied the number of days, i.e.

563 $n=20*8=160$ for the 3h precipitation forecast, and $n=20$ for the daily precipitation forecast.

564 Indicating the contingency tables by the vector $\boldsymbol{x}$:

565 $$\boldsymbol{x}_{i,j} = (a,b,c,d)_{i,j} \tag{A2}$$

566 where i is the competing model ($i=1$ for CNTRL, $i=2$ for F3HA6) and j is the contingency table ($j=$

567 $1,\ldots,180$ for 3h forecast, and $j=1,\ldots,20$ for daily precipitation), the scores are computed from the

568 sum of the contingency tables:

569 $$S_i = f\left(\sum_{j=1}^{n} x_{i,j}\right) \tag{A3}$$

570 and the test statistic is given by the difference between S_1 and S_2.

571 The bootstrap method is applied by resampling the contingency tables in a consistent way. For this

572 purpose, a random number I_j is generated, which can assume the values 1 or 2. If I_j is 1 the

573 contingency table of CNTRL is selected, if I_j eq 2 the F3HA6 table is selected. The process is

574   repeated for each contingency table (j=1,…,180 for 3h forecast, and j=1,…,20 for daily

575   precipitation) and the scores S_1^* and S_2^* are computed:

576
$$S_1^* = f\left(\sum_{j=1}^{n} x_{I_j,j}\right); \quad S_2^* = f\left(\sum_{j=1}^{n} x_{3-I_j,j}\right) \tag{A4}$$

577   So, the two j-th contingency tables are swapped if I_j=2, while the swapping is not performed for

578   I_j=1.

579   This random sampling is performed a large number of times (10.000 in this paper). Each time the

580   scores are computed from the sum of the elements of the resampled contingency tables, Eqn. (A4),

581   to make the null distribution (S_1^*-S_2^*) of the difference between the scores of the competing

582   forecasts.

583   Then we compute the t_L and t_U that represent the $\alpha/2$ and $(1-\alpha)/2$ percentile of the null distribution

584   (S_1^*-S_2^*). The null hypothesis that the score difference between the two competing forecasts is zero

585   is rejected at the level 90 % (α=0.1) or 95% (α=0.05) if:

586
$$(S_1 - S_2) < t_L \quad \text{or} \quad (S_1 - S_2) > t_U \tag{A5}$$

587   where S_1 and S_2 are the generic scores of the actual distributions (not resampled).

588

589   **Acknowledgments**

590   This work is a contribution to the HyMeX program. The author acknowledges Meteo-France and

591   the HyMeX program for supplying the data, sponsored by Grants MISTRALS/HyMeX and ANR-

592   11-BS56-0005 IODA-MED project. The ECMWF and Aeronautica Militare – CNMCA are

593   acknowledged for the access to the MARS database. LINET data were provided by Nowcast GmbH

594   (https://www.nowcast.de/) within a scientific agreement between Prof. H.-D. Betz and the Satellite

595   Meteorological Group of CNR-ISAC in Rome.

596

597   **References**

598   Accadia, C., S. Mariani, M. Casaioli, A. Lavagnini Sensitivity of precipitation forecast skill scores
599   to bilinear interpolation and a simple nearest-neighbor average method on high-resolution
600   verification grids, Weather Forecast., 18 (2003), pp. 918–932

601   Alexander, G.D., Weinman, J.A., Karyampoudi, V.M., Olson, W.S., Lee, A.C.L., 1999. The effect
602   of assimilating rain rates derived from satellites and lightning on forecasts of the 1993 superstorm.
603   Mon. Weather Rev. 127, 1433 - 1457.

604 Betz, H. D., Schmidt, K., Laroche, P., Blanchet, P., Oettinger, W. P., Defer, E., Dziewit, Z.,
605 Konarski, J., 2009. LINET—An in- ternational lightning detection network in Europe. Atmos. Res.,
606 91, 564–573.

607 Casaioli, M., Coraci, E., Mariani, S., Ferrario, M. E., Sansone, M., Davolio, S., Cordella, M.,
608 Manzato, A., Pucillo, A., and Bajo, M.: The impact of different NWP forecasting systems on acqua
609 alta forecasts: two IOP case studies over the NEI target site, 7th HyMeX Workshop, 7–10 October
610 2013, Cassis, France, 2013.

611 Chang, D.E., Weinman, J.A., Morales, C.A., Olson, W.S., 2001. The effect of spaceborn
612 microwave and ground-based continuous lightning measurements on forecasts of the 1998
613 Groundhog Day storm. Mon. Weather Rev. 129, 1809-1833.

614 Chen, C., Cotton, W. R., 1983. A One-Dimensional Simulation of the Stratocumulus-Capped
615 Mixed Layer. The Boundary Layer Meteorology 25, 289–321.

616 Cotton, W. R., Pielke, R. A. Sr., Walko, R. L., Liston, G. E., Tremback, C. J., Jiang, H., McAnelly,
617 R. L., Harrington, J. Y., Nicholls, M. E. , Carrio, C. G., McFadden, J. P., 2003. RAMS 2001:
618 Current status and future directions. Meteorological and Atmospheric Physics 82, 5-29.

619 Dahl, J. M. L., Holler, H., Schumann, U., 2011: Modeling the flash rate of thunderstorms. Part II:
620 Implementation. Mon. Wea. Rev., 139, 3112–3124.

621 Davolio, S., Ferretti,R., Baldini, L., Casaioli, M., Cimini,D., Ferrario, M. E. Enrico, Gentile, S.,
622 Loglisci, N., Maiello, I., Manzato, A., Mariani, S., Marsigli, C., Marzano, F. S., Miglietta, M. M.,
623 Montani, A., Panegrossi, G., Pasi, F., Pichelli, E., Pucillo, A., Zinzi, A.: The role of the Italian
624 scientific community in the first HyMeX SOP: an outstanding multidisciplinary experience.
625 Meteorologische Zeitschrift Vol. 24 No. 3, p. 261 – 267, 2015.

626 Drobinski, P., V. Ducrocq, P. Alpert, E. Anagnostou, K. Béranger, M. Borga, I. Braud, A. Chanzy,
627 S. Davolio, G. Delrieu, C. Estournel, N. Filali Boubrahmi, J. Font, V. Grubisic, S. Gualdi, V.
628 Homar, B. Ivancan-Picek, C. Kottmeier, V. Kotroni, K. Lagouvardos, P. Lionello, M.C. Llasat, W.
629 Ludwig, C. Lutoff, A. Mariotti, E. Richard, R. Romero, R. Rotunno, O. Roussot, I. Ruin, S. Somot,
630 I. Taupier-Letage, J. Tintore, R. Uijlenhoet, H. Wernli, 2014: HyMeX, a 10-year multidisciplinary
631 program on the Mediterranean water cycle. Bull. Amer. Meteor. Soc. 95, 1063–1082,
632 doi:10.1175/BAMS-D-12-00242.1.

633 Ducrocq, V., I. Braud, S. Davolio, R. Ferretti, C. Flamant, A. Jansa, N. Kalthoff, E. Richard, I.
634 Taupier-Letage, P.A. Ayral, S. Belamari, A. Berne, M. Borga, B. Boudevillain, O. Bock, J.-L.
635 Boichard, M.-N. Bouin, O. Bousquet, C. Bouvier, J. Chiggiato, D. Cimini, U. Corsmeier, L.
636 Coppola, P. Cocquerez, E. Defer, P. Drobinski, Y. Dufournet, N. Fourrié, J.J. Gourley, L. Labatut,
637 D. Lambert, J. Le Coz, F.S. Marzano, G. Molinié, A. Montani, G. Nord, M. Nuret, K. Ramage, B.
638 Rison, O. Roussot, F. Said, A. Schwarzenboeck, P. Testor, J. Van Baelen, B. Vincendon, M. Aran,
639 J. Tamayo, 2014: HyMeX-SOP1, the field campaign dedicated to heavy precipitation and flash
640 flooding in the northwestern Mediterranean. Bull. Amer. Meteor. Soc. 95, 1083–1100,
641 doi:10.1175/BAMS-D-12-00244.1.

642 Federico, S., 2016: Implementation of the WSM5 and WSM6 single moment microphysics scheme
643 into the RAMS model: verification for the HyMeX-SOP1, Advances in Meteorology.
644 Volume 2016 (2016), Article ID 5094126, 17 pages http://dx.doi.org/10.1155/2016/5094126.

645 Federico, S., Avolio, E., Petracca, M., Panegrossi, G., Sanò, P., Casella, D., Dietrich, S., 2014:
646 Simulating lightning into the RAMS model: implementation and preliminary results, Nat. Hazards
647 Earth Syst. Sci., i14, 2933-2950. doi:10.5194/nhess-14-2933-2014.

648 Federico, S., Avolio, E., Bellecci, C., Colacino, M., 2003. On the performance of a limited area
649 model for quantitative precipitation forecast over Calabria. *Il Nuovo Cimento C* , **26 C**, 663-676.

Federico, S., Petracca, M., Panegrossi, G., and Dietrich, 2016: Improvement of RAMS precipitation forecast at the short-range through lightning data assimilation. Nat. Hazards Earth Syst. Sci. Discuss., doi:10.5194/nhess-2016-291.

Ferretti, R., E. Pichelli, S. Gentile, I. Maiello, D. Cimini, S. Davolio, M.M. Miglietta, G. Panegrossi, L. Baldini, F. Pasi, F.S. Marzano, A. Zinzi, S. Mariani, M. Casaioli, G. Bartolini, N. Loglisci, A. Montani, C. Marsigli, A. Manzato, A. Pucillo, M.E. Ferrario, V. Colaiuda, R. Rotunno, 2014: Overview of the first HyMeX Special Observation Period over Italy: observations and model results. Hydrol. Earth Syst. Sc. 18, 1953–1977, 2014.

Fierro, A. O., Gao, J., Ziegler, C. L., Mansell, E. R., Macgorman, D. R., Dembek, S. R., 2013: Evaluation of a cloud scale lightning data assimilation technique and a 3DVAR method for the analysis and short-term forecast of the 29 June 2012 derecho event. Mon. Weather Rev. doi: http://dx.doi.org/10.1175/MWR-D-13-00142.1

Giannaros, T. M., Kotroni, V., Lagouvardos, K., 2016: WRF-LTNGDA: A lightning data assimilation technique implemented in the WRF model for improving precipitation forecasts Environmental Modelling & Software 76 (2016) 54-68. http://dx.doi.org/10.1016/j.envsoft.2015.11.017.

Goodman, S.J., Buechler, D.E., Wright, P.D., Rust, W.D., 1988. Lightning and precipitation history of a microburst-producing storm. Geophys. Res. Lett. 15, 1185-1188.

Hamill, T. M.: Hypothesis tests for evaluating numerical precipitation forecasts Weather Forecast., 14 (1999), pp. 155–167.

Hodur, R.M., 1997. The naval research Laboratory's coupled Ocean/Atmosphere mesoscale prediction system (COAMPS). Mon. Weather. Rev. 125, 1414-1430.

Kain, J.S., Fritsch, J.M., 1993. Convective parameterization for mesoscale models: the Kain-Fritsch scheme. The representation of cumulus convection in numerical models, Meteor. Monogr. No. 46 Am. Meteor. Soc. 165e170.

Jansà, A., P. Alpert, P. Arbogast, A. Buzzi, B. Ivancan-Picek, V. Kotroni, M. C. Llasat, C. Ramis, E. Richard, R. Romero, and A. Speranza, "MEDEX: a general overview", Natural Hazards and Earth System Sciences, 14, 1965-1984, 2014.

Jones, C. D., and B. Macpherson, 1997: A latent heat nudging scheme for the assimilation of precipitation into an operational mesoscale model. Meteor. Appl., 4, 269–277.

Hong, S.Y., Lim, J.J.O., 2006. The WRF single-moment 6-class microphysics scheme (WSM6). J. Korean Meteorol. Soc. 42, 129–151.

Kuo, H. L., 1974. Further Studies of the Parameterization of the Influence of Cumulus Convection on Large-Scale Flow, J. Atmos. Sci., 31, 1232–1240.

Lagouvardos, K., Kotroni, V., Betz, H.D., Schmidt, K., 2009. A comparison of lightning data provided by ZEUS and LINET networks over Western Europe. Nat. Hazards Earth Syst. Sci. 9, 1713-1717.

Liu, C., K. Ikeda, G. Thompson, R. Rasmussen, and J. Dudhia, 2011: High-Resolution Simulations of Wintertime Precipitation in the Colorado Headwaters Region: Sensitivity to Physics Parameterizations. Mon. Wea. Rev., 139, 3533–3553. doi: http://dx.doi.org/10.1175/MWR-D-11-00009.1

MacGorman, D. R. and Rust, W. D.: 1998, The electrical nature of storms, Oxford University Press, USA.

Mansell, E.R., Ziegler, C.L., MacGorman, D.R., 2007. A lightning data assimilation technique for mesoscale forecast models. Mon. Weather Rev. 135, 1732e1748.

Manzato, A., S. Davolio, M. M. Miglietta, A. Pucillo, and M. Setvák, 2014: 12 September 2012: A supercell outbreak in NE Italy?. Atmos. Res., 153, 98-118.

Mariani, S., Casaioli, M., and Malguzzi, P.: Towards a new BOLAM-MOLOCH suite for the SIMM forecasting system: implementation of an optimised configuration for the HyMeX Special Observation Periods, Nat. Hazards Earth Syst. Sci. Discuss., 2, 649–680, doi:10.5194/nhessd-2-649-2014, 2014.

Molinari, J., Corsetti, T., 1985. Incorporation of cloud-scale and mesoscale down-drafts into a cumulus parametrization: results of one and three-dimensional integration. Mon. Wea. Rev. 113 (4), 485-501.

Papadopoulos, A., Chronis, T.G., Anagnostou, E.N., 2005. Improving convective precipitation forecasting through assimilation of regional lightning measure-ments in a mesoscale model. Mon. Weather Rev. 133, 1961-1977.

Pielke, R. A., 2002. Mesoscale Meteorological Modeling. Academic Press, San Diego. 676 pp.

Qie, X., Zhu, R., Yuan, T., Wu, X., Li, W., Liu, D., 2014. Application of total-lightning data assimilation in a mesoscale convective system based on the WRF model. Atmos. Res. 145e146, 255-266.

Smagorinsky, J., 1963. General circulation experiments with the primitive equations. Part I, The basic experiment. Mon. Wea. Rev. 91 (3), 99-164.

Stensrud, D. J., Fritsch, J. M., 1994: Mesoscale convective systems in weakly forced large-scale environments. Part II: Generation of a mesoscale initial condition. Mon. Wea. Rev., 122, 2068–2083.

Walko, R. L., Band, L. E., Baron, J., Kittel, T. G., Lammers, R., Lee, T. J., Ojima, D., Pielke, R. A. Sr., Taylor, C., Tague, C., Tremback, C. J., Vidale, P. L., 2000: Coupled Atmosphere-Biosphere-Hydrology Models for environmental prediction. Jou. App. Meteorol. 39 (6), 931-944.

Wilks, D. S., 2006. Statistical Methods in the Atmospheric Sciences", Academic Press, 627 pp.

Tables

Table 1: The twenty case studies.

Month	Days
September 2012	12,13,14,24,26,30
October 2012	12,13,15,26,27,28,29,31
November 2012	4,5,11,20,21,28

733

734

735

736

737

738 **Figures**

739

740

741

742
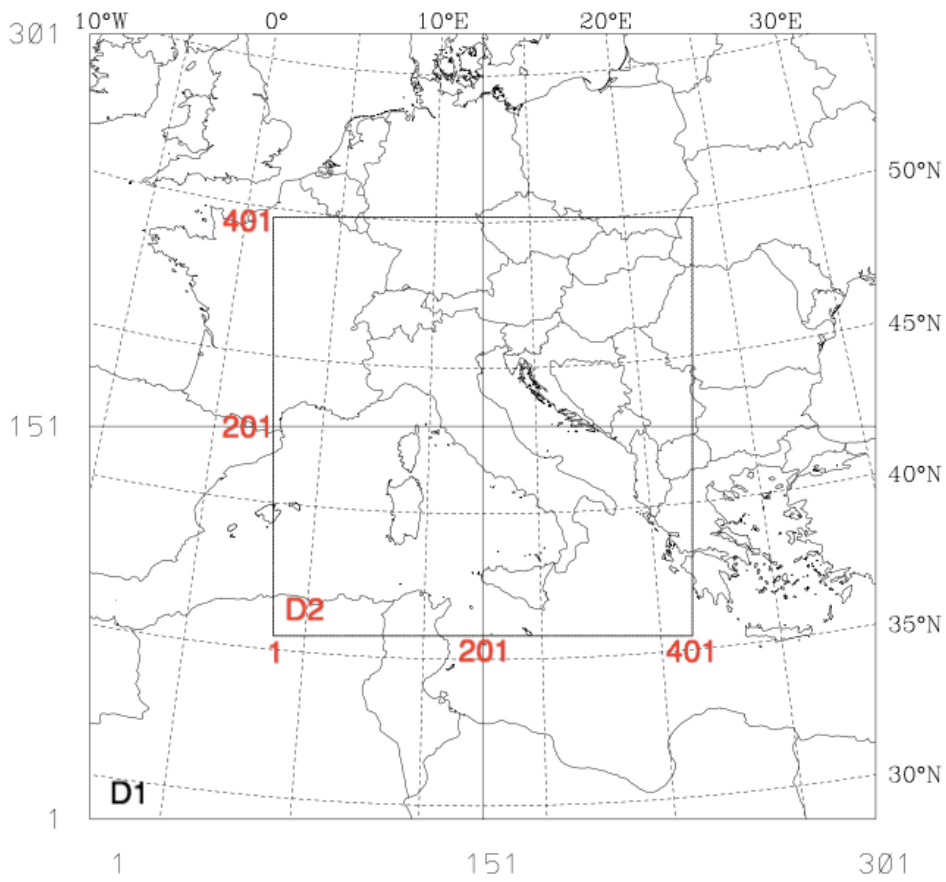
743 Figure 1: The two domains (D1, D2). D1 has 301 grid points in both the WE and SN directions; D2
744 has 401 grid points in both WE and SN directions.

745

746

747

748

749

750
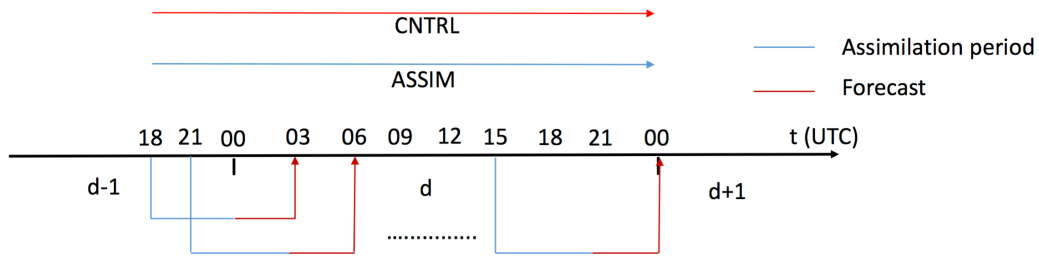
Figure 2: Synopsis of the simulations F3HA6 (below the timeline). The blue line is the assimilation stage, while the red line is the forecast stage; d, d+1 and d-1 are the actual day, the day after and the day before the actual day, respectively. In the upper part of the figure the CNTRL and ASSIM simulations are shown.

a)

757

758

759

b)
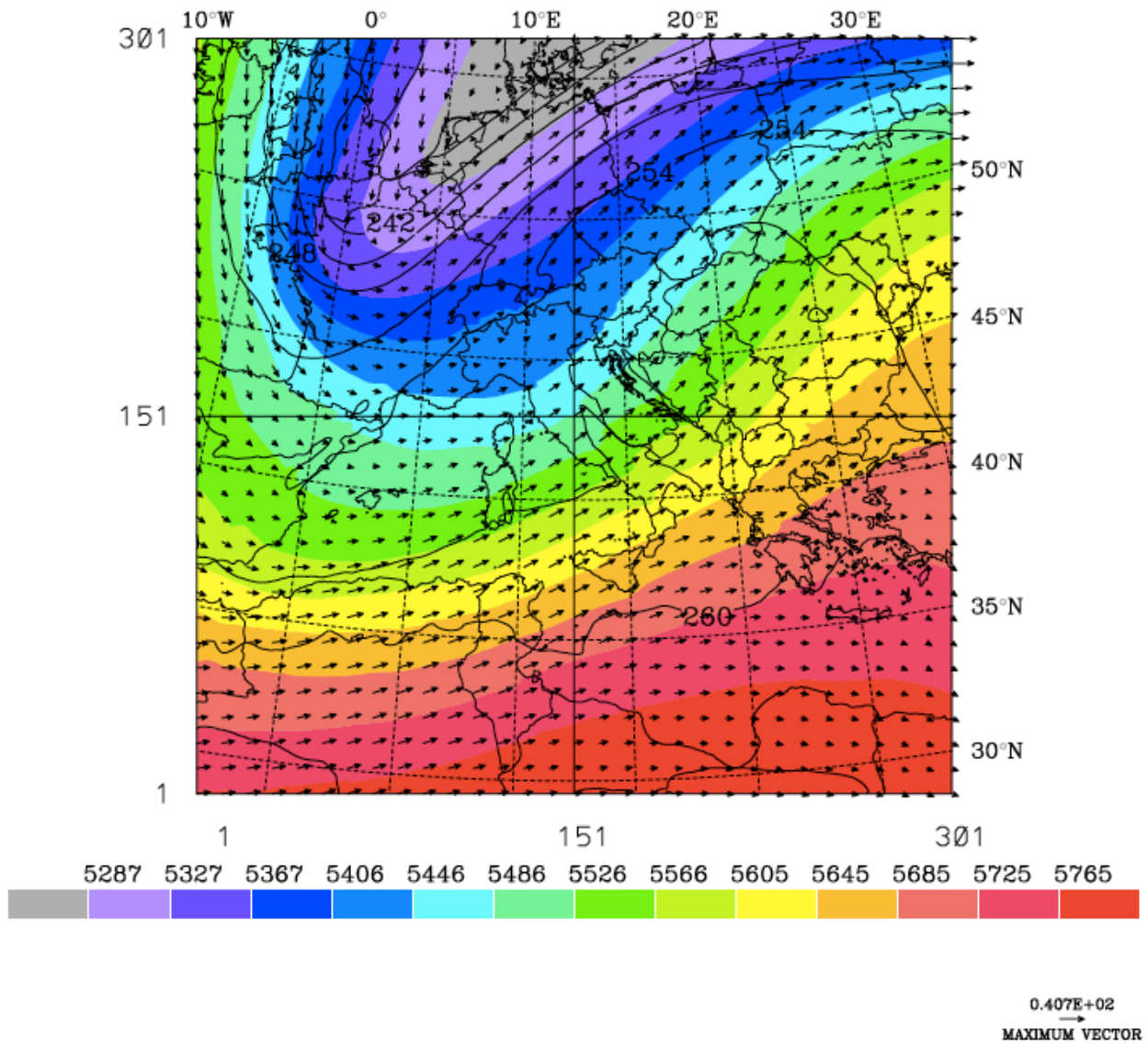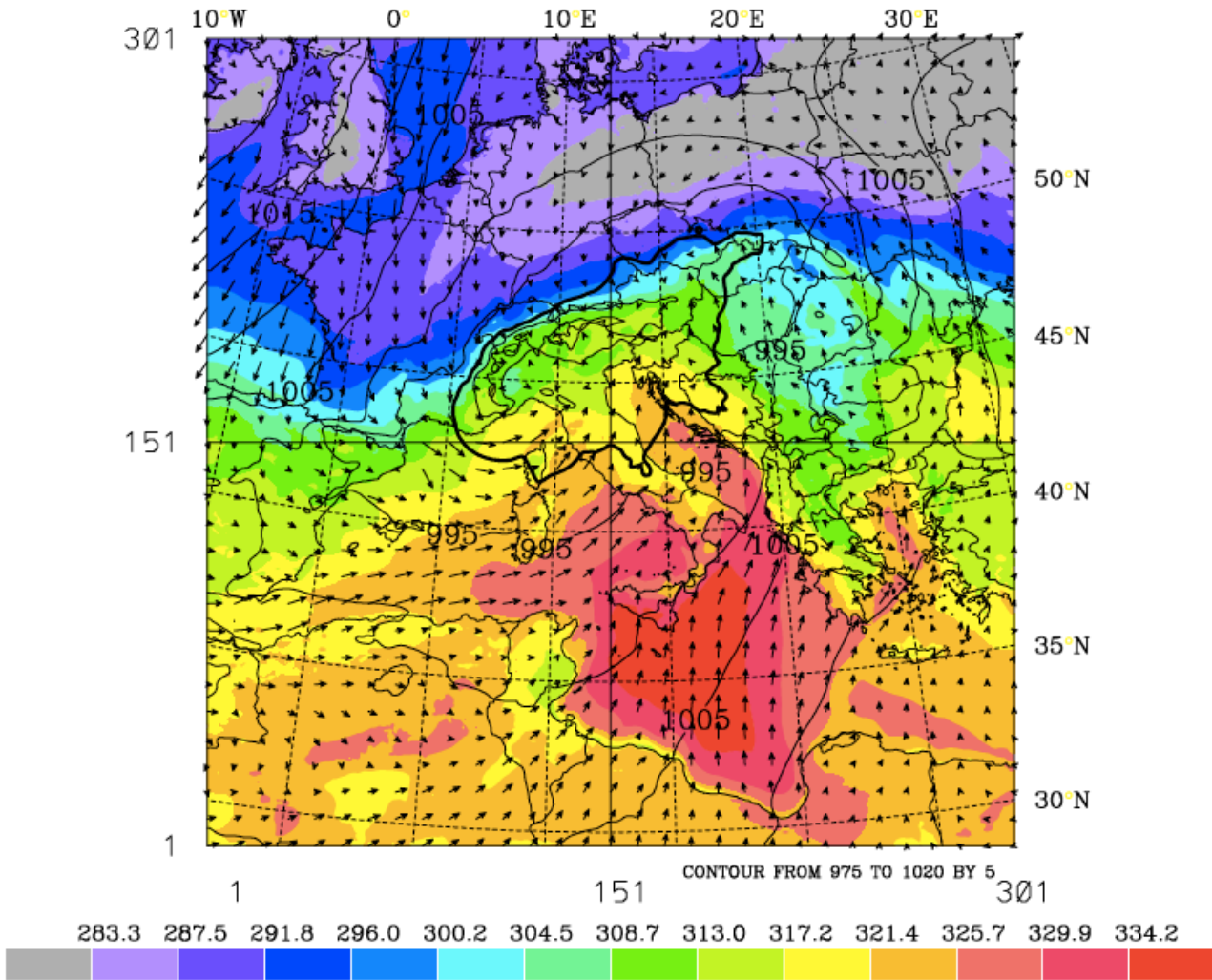
Figure 3: Synoptic situation at 12 UTC on 27 October 2012; a) 500 hPa: temperature (black contours from 236 K to 263 K every 3 K), geopotential height (filled contours, values shown by the colour bar at the bottom) and wind vectors (maximum wind value 41 m/s); b) surface: Sea level pressure (contour from 975 to 1020 hPa every 5 hPa, the thick line is the 990 hPa contour), equivalent potential temperature (filled contours, values shown by the colour bar at the bottom), and winds (maximum wind vector is 17 m/s) simulated at 25 m above the underlying surface in the terrain-following coordinates of RAMS. This figure is derived from the RAMS run at 10 km horizontal-resolution. The bottom and left axes show the grid point number, while the top and right axes show the geographical coordinates.

779   **a)**
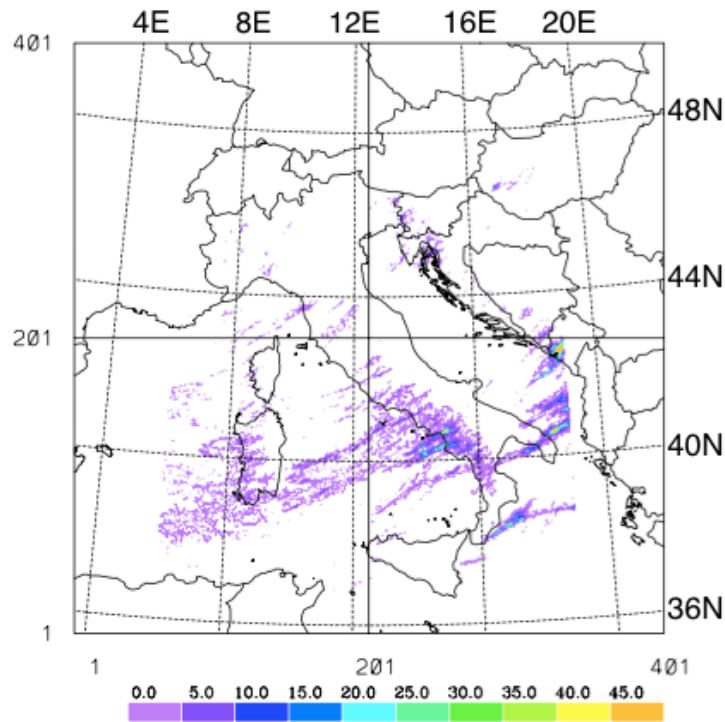
780

781

782   **b)**
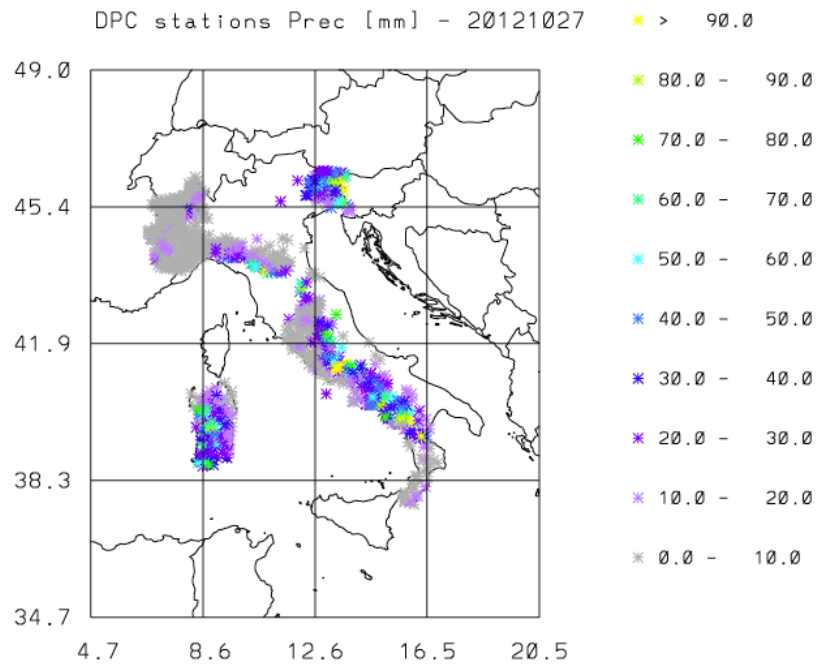
783

784   Figure 4: a) Lightning density on 27 October 2012 [number of flashes/16 km^2]. The lightning
785   number is obtained by remapping the lightning observed by LINET onto the RAMS grid at 4 km
786   horizontal resolution. Note that the lightning are cut on all sides (this is especially evident on the
787   Eastern bound) because of the data availability. The bottom and left axes show the grid point
788   number, while the top and right axes show the geographical coordinates; b) daily precipitation [mm]
789   recorded by available rain gauges on 27 October 2012.

790

791 **a)**
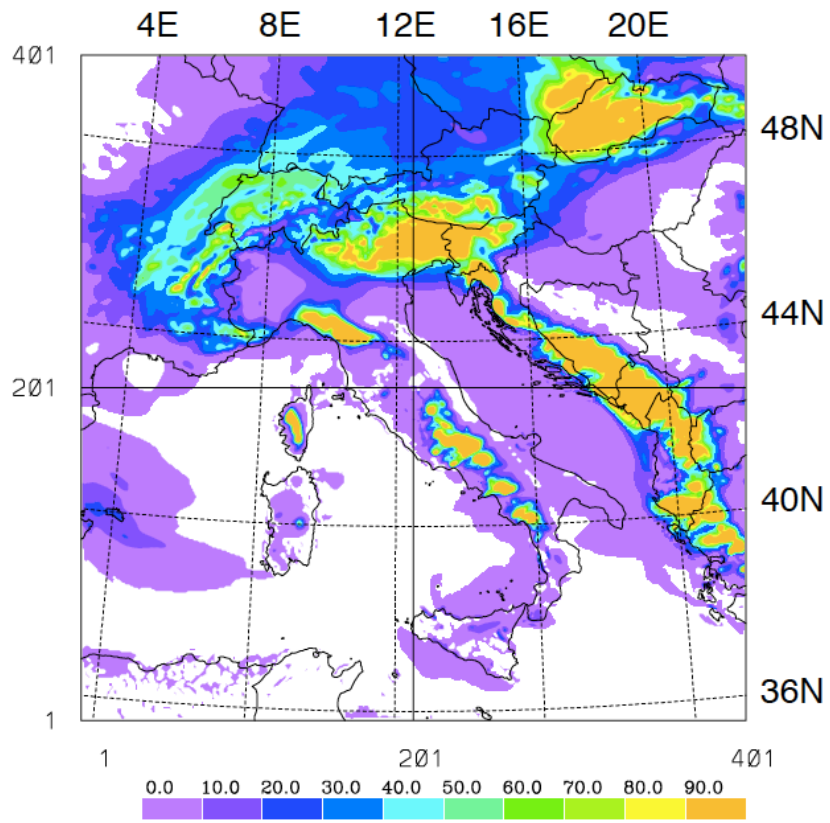
792
793

794 **b)**

795
796

c)
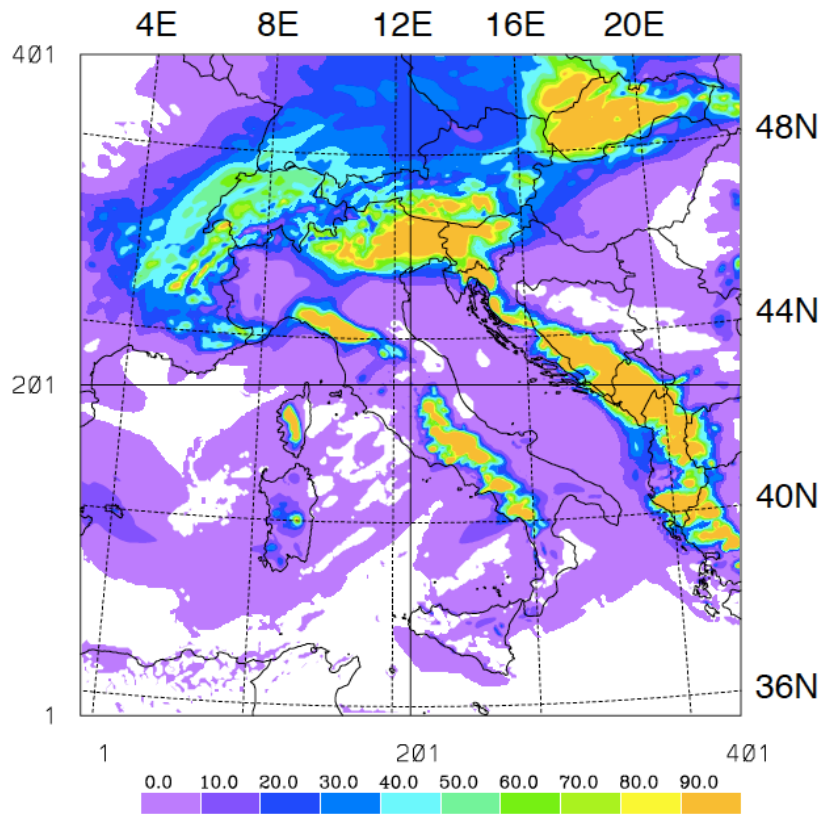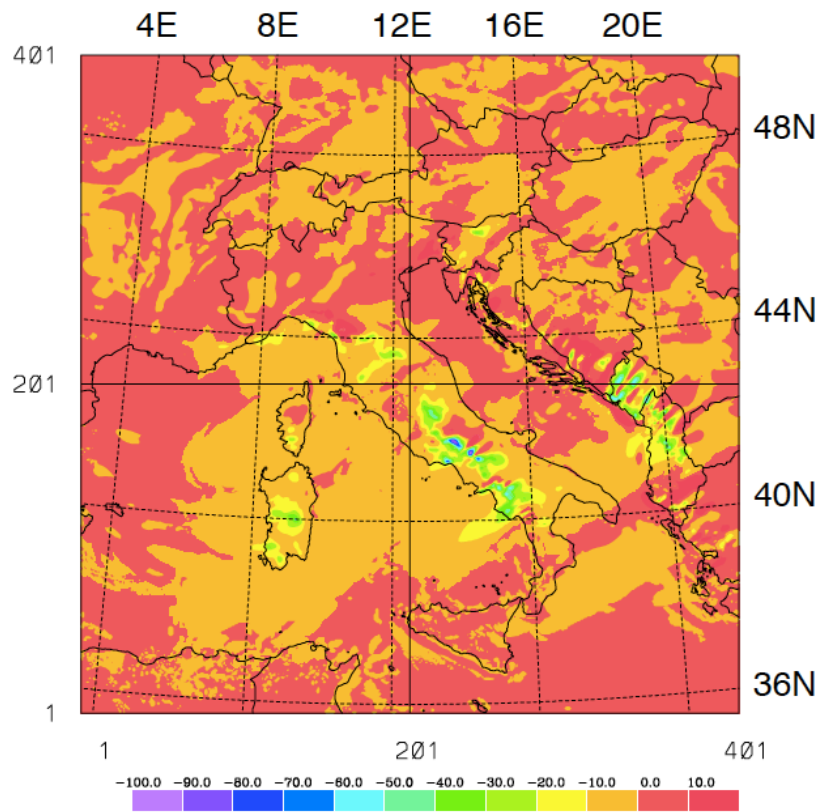
Figure 5: a) daily precipitation [mm] forecast of CNTRL (maximum value 300 mm in Southern Italy; over NE Italy the maximum value is 135 mm); b) daily precipitation [mm] forecast obtained by summing the eight 3h forecasts of F3HA6 (the maximum value is 320 mm in Southern Italy; over NE Italy the maximum simulated value is 132 mm); c) difference of daily precipitation [mm] between CNTRL and F3HA6.

819 **a)**
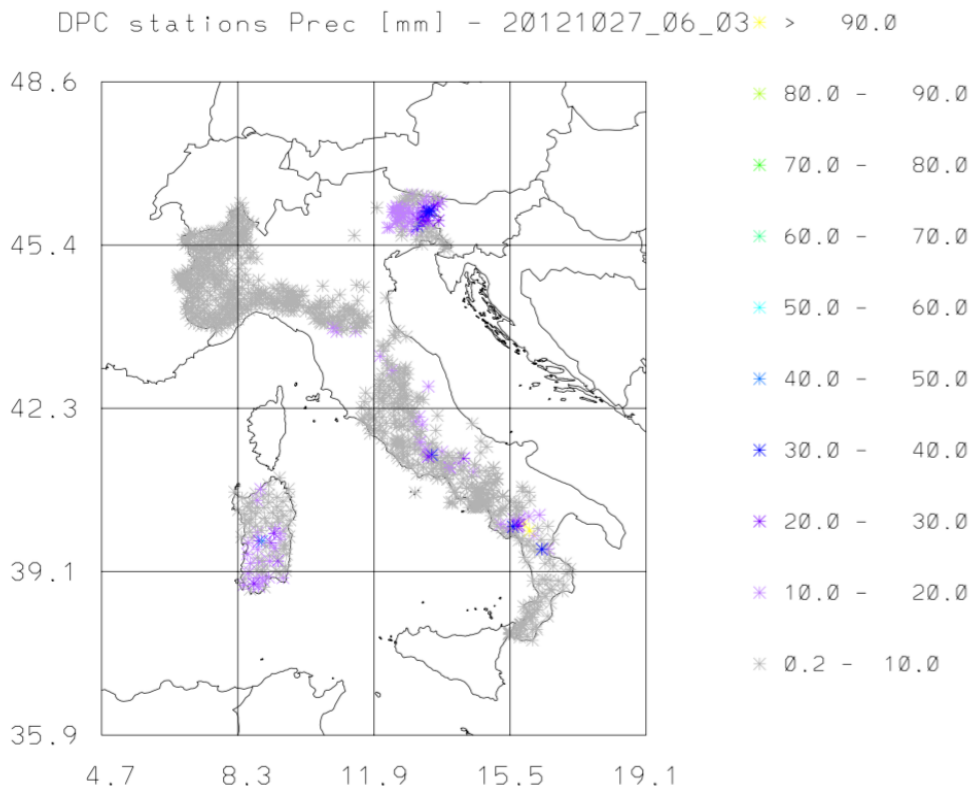
820

821

822 **b)**
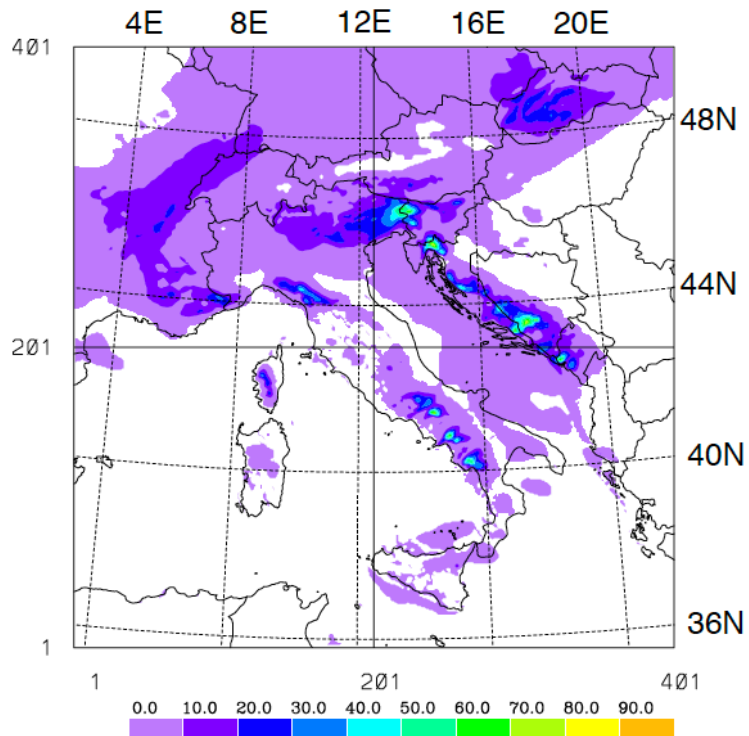
823

824

825 **c)**
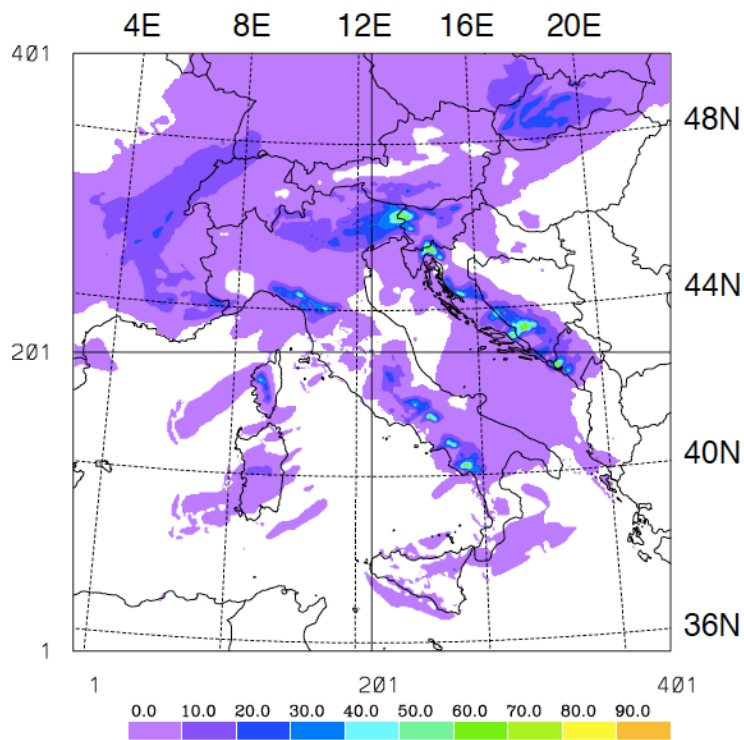
826

827

828 Figure 6: a) Precipitation [mm] recorded by raingauges between 06 and 09 UTC; b) As in a) for the
829 CNTRL forecast; c) As in a) for the F3HA6 forecast.

830

831

832

833

834

835

836

837

838

839

840

841

842

843

844

845

846

847

848

849   **a)**
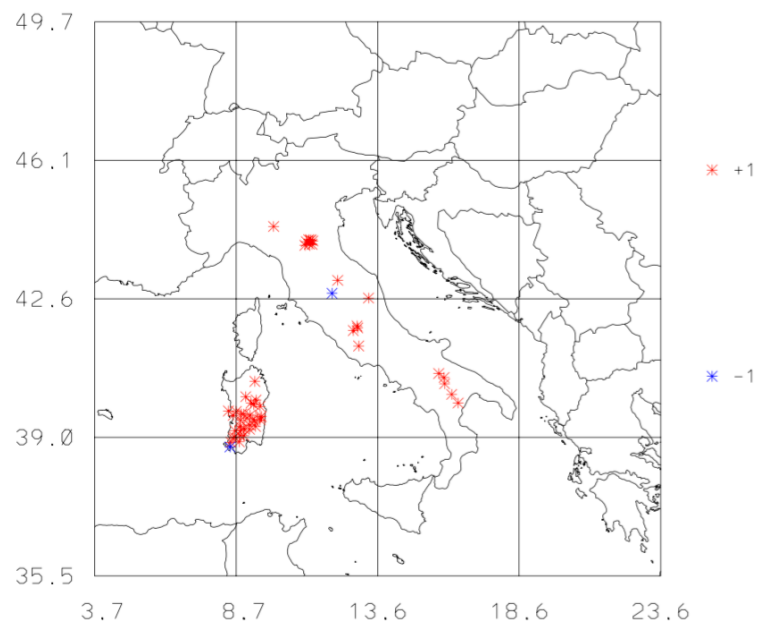
850

851

852   **b)**

853
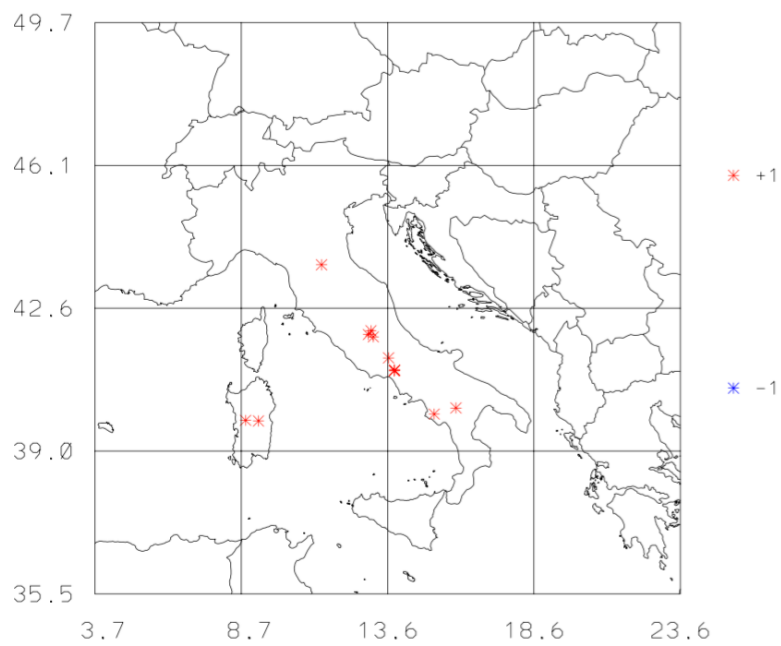
854

855   Figure 7: a) Difference between the hits of the contingency tables of F3HA6 and CNTRL for the 1
856   mm/3h (8 mm/day) forecast; b) As in a) for the 10 mm/3h (80 mm/day) threshold.

857

858

859

860

861 **a)**   **b)**

862
863
864
865
866 **c)**   **d)**
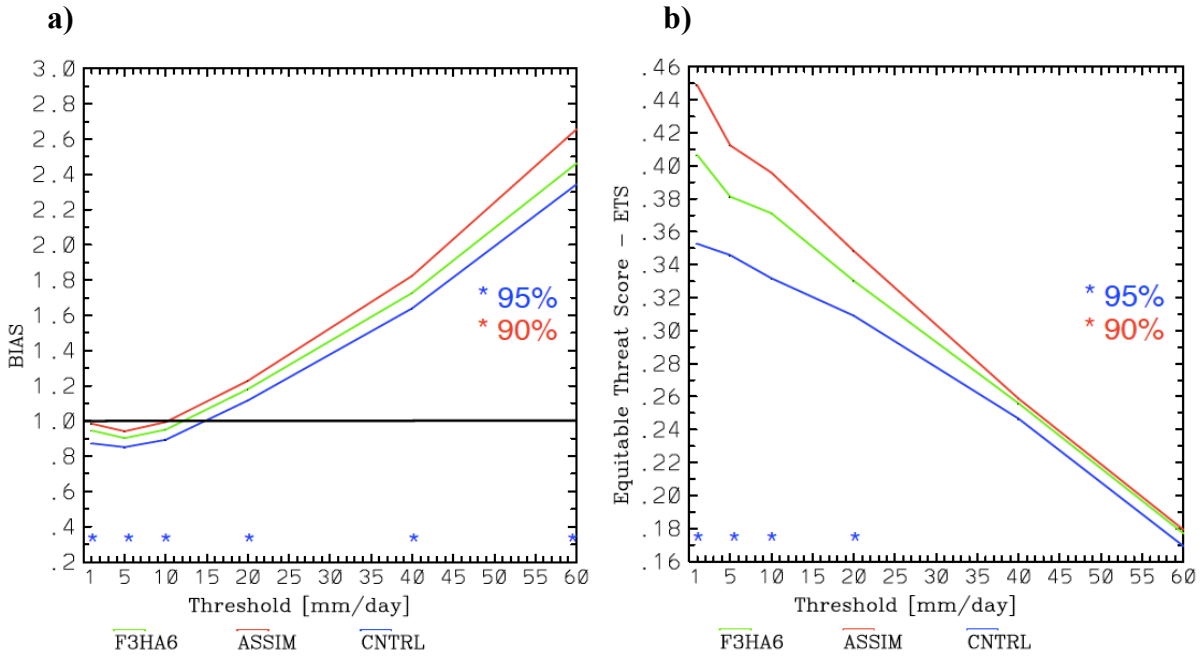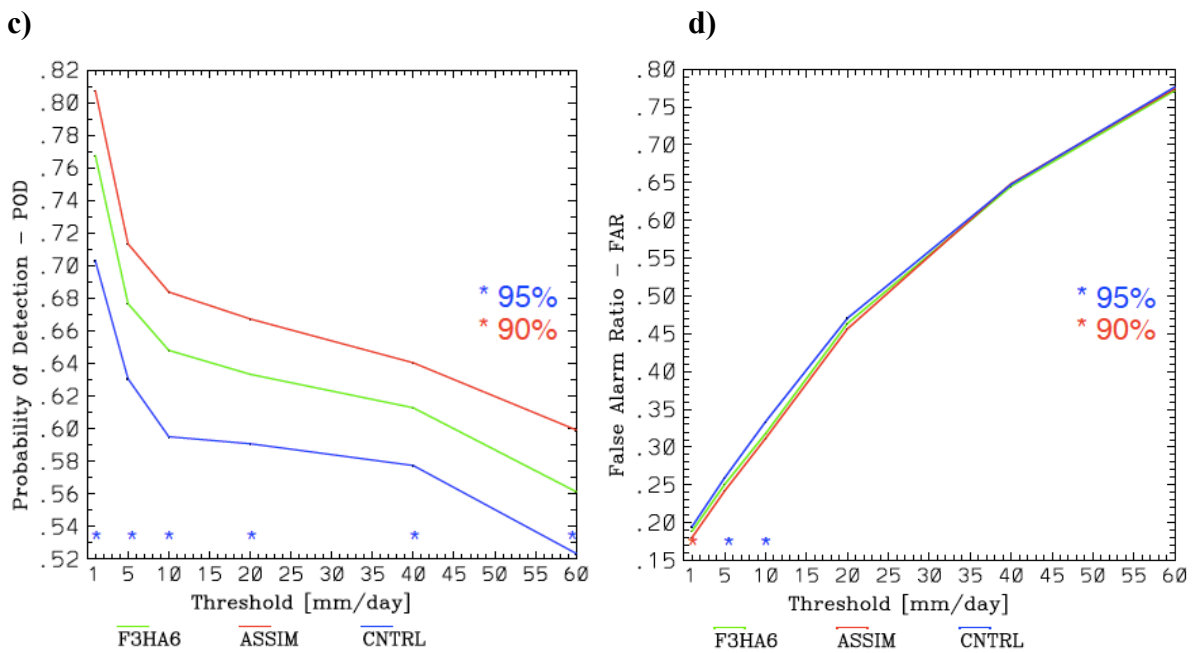
867
868 Figure 8: Scores for the daily precipitation computed by summing the contingency tables of all
869 twenty case studies; a) Bias (the line of the perfect score 1.0 is shown in black); b) Equitable Threat
870 Score; c) Probability of Detection; d) False Alarm Ratio. F3HA6 is in green, ASSIM is in red and
871 CNTRL in blue. The asterisks above the x-axis show the results of the hypothesis testing (95%
872 blue, 90% red) of the difference between F3HA6 and CNTRL scores.

873
874
875
876

877 **a)**

878
879
880
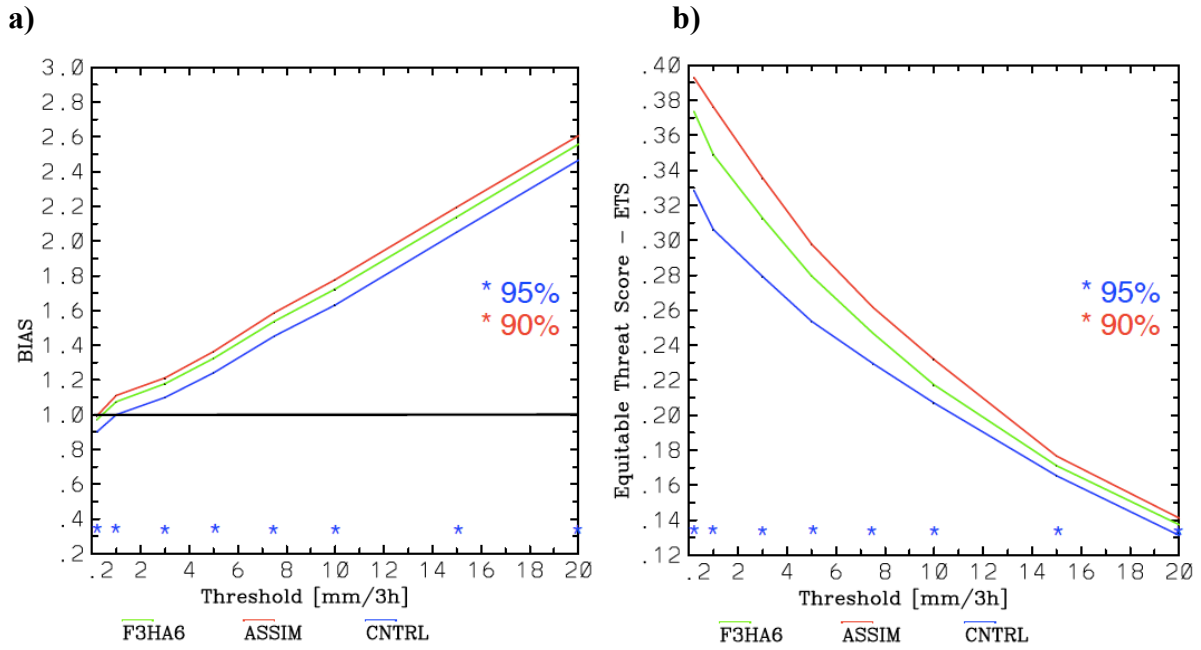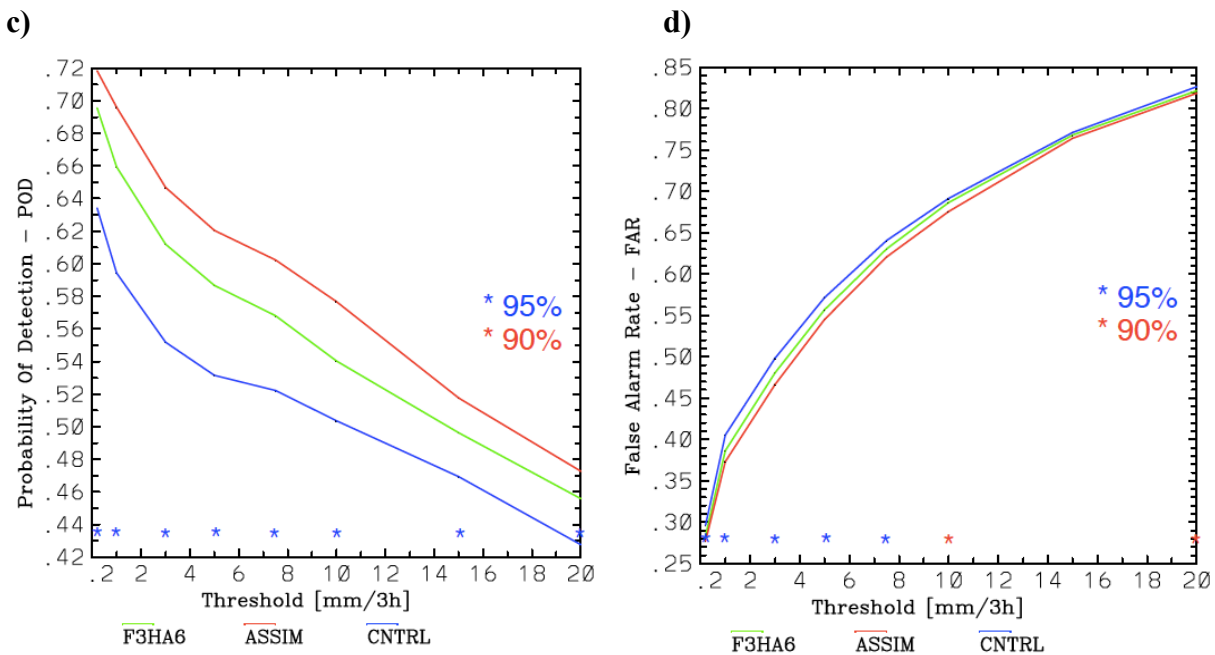
883 Figure 9: Scores for the 3h precipitation computed by summing the 160 contingency tables of the
884 twenty case studies; a) Bias (the line of the perfect score 1.0 is shown in black); b) Equitable Threat
885 Score; c) Probability of Detection; d) False Alarm Ratio. F3HA6 is in green, ASSIM is in red and
886 CNTRL in blue. The asterisks above the x-axis show the results of the hypothesis testing (95%
887 blue, 90% red) of the difference between F3HA6 and CNTRL scores.